LETTERS
PUBLISHED ONLINE: 24 AUGUST 2014 | DOI: 10.1038/NNANO.2014.167
nature nanotechnology

Ultrafast charge transfer in atomically thin MoS_2/WS_2 heterostructures

Xiaoping Hong[1†], Jonghwan Kim[1†], Su-Fei Shi[1,2†], Yu Zhang[3], Chenhao Jin[1], Yinghui Sun[1], Sefaattin Tongay[2,4,5], Junqiao Wu[2,4], Yanfeng Zhang[3] and Feng Wang[1,2,6*]

Van der Waals heterostructures have recently emerged as a new class of materials, where quantum coupling between stacked atomically thin two-dimensional layers, including graphene, hexagonal-boron nitride and transition-metal dichalcogenides (MX_2), give rise to fascinating new phenomena[1–10]. MX_2 heterostructures are particularly exciting for novel optoelectronic and photovoltaic applications, because two-dimensional MX_2 monolayers can have an optical bandgap in the near-infrared to visible spectral range and exhibit extremely strong light–matter interactions[2,3,11]. Theory predicts that many stacked MX_2 heterostructures form type II semiconductor heterojunctions that facilitate efficient electron–hole separation for light detection and harvesting[12–16]. Here, we report the first experimental observation of ultrafast charge transfer in photoexcited MoS_2/WS_2 heterostructures using both photoluminescence mapping and femtosecond pump–probe spectroscopy. We show that hole transfer from the MoS_2 layer to the WS_2 layer takes place within 50 fs after optical excitation, a remarkable rate for van der Waals coupled two-dimensional layers. Such ultrafast charge transfer in van der Waals heterostructures can enable novel two-dimensional devices for optoelectronics and light harvesting.

Atomically thin two-dimensional crystals constitute a rich family of materials ranging from insulators and semiconductors to semimetals and superconductors[1]. Heterostructures from these two-dimensional materials offer a new platform for exploring new physics (for example, superlattice Dirac points[4] and Hofstadter butterfly pattern[5–7]) and new devices (such as tunnelling transistors[8], memory devices[9] and ultrathin photodetectors[2,3]). Van der Waals heterostructures of semiconducting MX_2 layers are particularly exciting for optoelectronic and light-harvesting applications, because many MX_2 monolayers are direct-bandgap semiconductors[17,18] with remarkably strong light–matter interactions[2,3,11]. Importantly, MX_2 heterostructures are predicted to form type II heterojunctions, which can assist in the efficient separation of photoexcited electrons and holes[12–15].

In type II heterojunctions, the conduction band minimum and valence band maximum reside in two separate materials. Photoexcited electrons and holes therefore prefer to stay at separate locations. Figure 1a illustrates the alignment of electronic bands of MoS_2 and WS_2 monolayers as predicted by a recent theory[12]. It shows that monolayer MoS_2 and WS_2 have bandgaps of 2.39 eV and 2.31 eV, respectively, and the MoS_2 valence band maximum is 350 meV lower than that of WS_2. Consequently, the MoS_2/WS_2 heterostructure forms a type II heterojunction (if we neglect the hybridization of electronic states in the MoS_2 and WS_2 layers), with the conduction band minimum residing in MoS_2 and the valence band maximum in WS_2, respectively (Supplementary Sections 1 and 2). In the single-particle picture this heterojunction structure will lead to efficient charge transfer, with separated electrons and holes residing in two layers upon optical excitation (Fig. 1a), a scenario that can have a dominating effect on both light emission and photovoltaic responses in MoS_2/WS_2 heterostructures.

However, there are two outstanding questions regarding charge transfer processes in the atomically thin and van der Waals-coupled MoS_2/WS_2 heterostructure: (1) How do strong electron–electron interactions and excitonic effects affect charge transfer processes? and (2) How fast can charge transfer take place between van der Waals-coupled layers? Electron–electron interactions are dramatically enhanced in two-dimensional materials due both to size confinement and inefficient screening. Theoretical studies[19,20] have predicted an exciton binding energy from 500 meV to 1 eV in MX_2 monolayers, which is larger than the expected band displacement of 350 meV in the MoS_2/WS_2 heterostructure. Accordingly, the exciton cannot dissociate into a free electron and a free hole in two separate layers. Will this large exciton binding energy then prevent charge transfer processes and keep the exciton in one layer, or will a new bound state of layer-separated electron and hole pair be generated? In addition, van der Waals coupling is rather weak compared to covalent bonding. Will that lead to a much slower charge transfer process in van der Waals heterostructures than in their covalent counterparts? Previous studies in organic photovoltaics (OPV)[21–24] have shown that ultrafast charge transfer and separation can take place in organic/organic van der Waals coupled interfaces. However, the two-dimensional MX_2 heterostructures possess two-dimensional crystalline structures and atomically sharp interfaces, which is fundamentally different from OPV molecular systems. So far, little is known about the ultrafast charge transfer dynamics in these new two-dimensional heterostructures. In this Letter, we study charge transfer dynamics in MoS_2/WS_2 heterolayers experimentally. Through combined photoluminescence spectroscopy and optical pump–probe spectroscopy, we demonstrate that ultrafast charge transfer takes place very efficiently in MoS_2/WS_2 heterostructures. In particular, holes in the MoS_2 layer can separate into the WS_2 layer within 50 fs upon photoexcitation.

Figure 1b schematically shows the sample configuration. In brief, MoS_2 monolayers were grown on 285 nm SiO_2/Si substrates using the chemical vapour deposition (CVD) method[25]. They were

[1]Department of Physics, University of California at Berkeley, Berkeley, California 94720, USA, [2]Materials Science Division, Lawrence Berkeley National Laboratory, Berkeley, California 94720, USA, [3]Department of Materials Science and Engineering, College of Engineering, Peking University, Beijing 100871, China, [4]Department of Materials Science and Engineering, University of California, Berkeley, California 94720-1760, USA, [5]School for Engineering of Matter, Transport and Energy, Arizona State University, Tempe, Arizona 85287, USA, [6]Kavli Energy NanoSciences Institute at the University of California, Berkeley and the Lawrence Berkeley National Laboratory, Berkeley, California 94720, USA, †These authors contributed equally to this work.
*e-mail: fengwang76@berkeley.edu

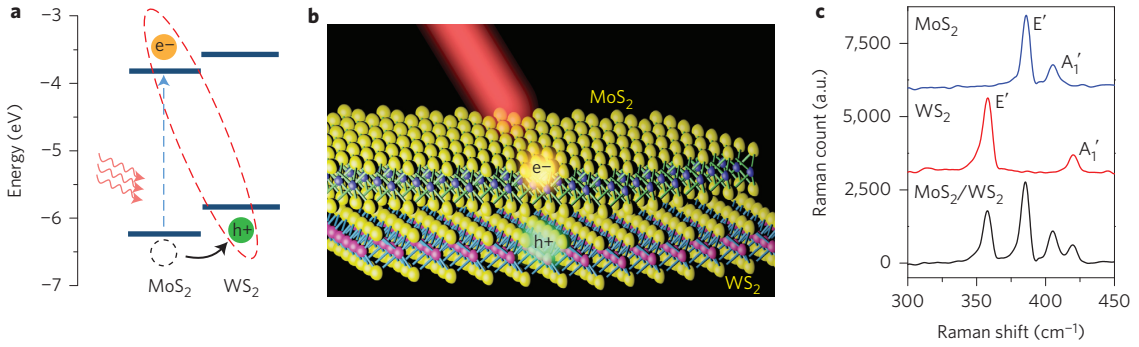

Figure 1 | Band alignment and structure of MoS_2/WS_2 heterostructures. a, Schematic of the theoretically predicted band alignment of a MoS_2/WS_2 heterostructure, which forms a type II heterojunction. Optical excitation of the MoS_2 A-exciton will lead to layer-separated electron (e^-) and hole (h^+) carriers. **b**, Illustration of a MoS_2/WS_2 heterostructure with a MoS_2 monolayer lying on top of a WS_2 monolayer. Electrons and holes created by light are shown to separate into different layers. **c**, Raman spectra of an isolated MoS_2 monolayer (blue trace), an isolated WS_2 monolayer (red trace) and a MoS_2/WS_2 heterostructure (black trace).

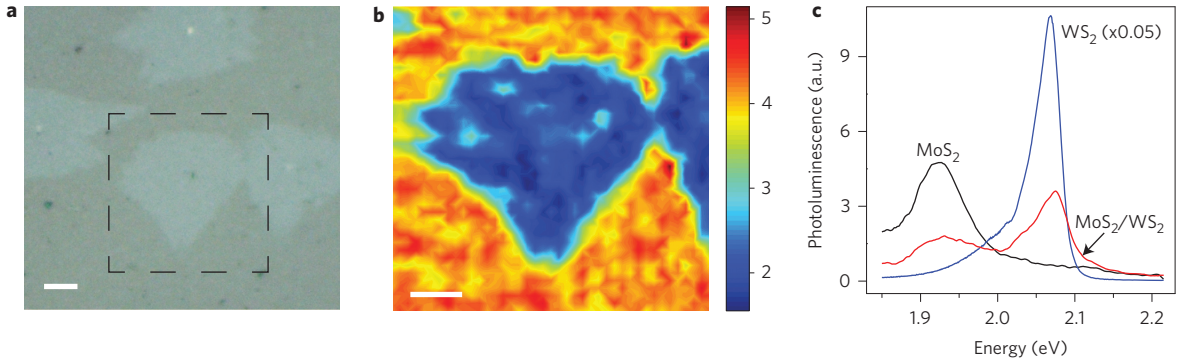

Figure 2 | Photoluminescence spectra and mapping of MoS_2/WS_2 heterostructures at 77 K. a, Optical microscope image of a typical MoS_2/WS_2 heterostructure sample. The MoS_2 layer covers the entire image and bright areas correspond to MoS_2/WS_2 heterostructures. Scale bar, 5 μm. **b**, Photoluminescence mapping data taken in the area within the dashed rectangle in **a**. The colour scale represents photoluminescence intensity at the MoS_2 A-exciton resonance (1.93 eV). It clearly shows that MoS_2 photoluminescence is strongly quenched in the heterostructure. Scale bar, 5 μm. **c**, Typical photoluminescence spectra of an isolated monolayer MoS_2, an isolated monolayer WS_2 and a MoS_2/WS_2 heterostructure. The isolated MoS_2 and WS_2 monolayers show strong photoluminescence at 1.93 eV and 2.06 eV, respectively, corresponding to their A-exciton resonances. Both exciton photoluminescence signals are strongly quenched in the MoS_2/WS_2 heterostructure, suggesting an efficient charge transfer process exists in the heterostructure.

subsequently transferred on top of as-grown CVD WS_2 flakes on sapphire substrates[26–30] to form MoS_2/WS_2 heterostructures. Raman spectra (Fig. 1c) from isolated MoS_2 and WS_2 films confirm that both are monolayers, because the energy separation between Raman active modes agrees well with previously reported values for monolayer MoS_2 and WS_2 (refs 27–30). The Raman spectrum of a MoS_2/WS_2 heterostructure (Fig. 1c) appears to comprise the addition of Raman modes from the constituent layers (see Supplementary Section 3 for a comparison of before and after annealing).

One sensitive probe of charge transfer in MX_2 heterostructures is photoluminescence spectroscopy, because an electron and hole pair spatially separated in two MX_2 layers cannot emit efficiently. We performed photoluminescence spectroscopy and mapping on multiple MoS_2/WS_2 heterostructure samples. Figure 2a presents an optical image of one sample, in which a large continuous MoS_2 piece (covering the entire image) has been transferred on top of WS_2 flakes (the bright areas). Figure 2b shows the photoluminescence intensity map at the MoS_2 A-exciton resonance (1.93 eV) at 77 K when the sample is excited by 2.33 eV photons. We observed strong photoluminescence signals in the MoS_2-only region, but the photoluminescence is significantly quenched in the MoS_2/WS_2 heterostructure region. Figure 2c further displays typical photoluminescence spectra for MoS_2/WS_2 heterostructures, isolated MoS_2 and isolated WS_2 layers with 2.33 eV excitation. It is apparent that MoS_2 and WS_2 monolayers show strong photoluminescence at their respective A-exciton resonances (1.93 eV and 2.06 eV), but both photoluminescence signals are efficiently quenched in MoS_2/WS_2 heterostructures. Room-temperature photoluminescence spectra also exhibit similar behaviour (Supplementary Section 4). In principle, photoluminescence signals can be quenched by two mechanisms in a heterostructure: energy transfer and charge transfer. However, energy transfer quenches only the photoluminescence from a higher energy transition (that is, 2.06 eV resonance in WS_2), and tends to enhance luminescence from the lower energy transition (1.93 eV resonance in MoS_2). On the other hand, charge transfer will quench light emission from all transitions. Accordingly, the observation of reduced photoluminescence from both WS_2 and MoS_2 exciton resonances in MoS_2/WS_2 heterostructures demonstrates that efficient charge transfer takes place in this type II heterojunction.

To directly probe the charge transfer process and its ultrafast dynamics, we measured transient absorption spectra of MoS_2/WS_2 heterostructures using resonant pump–probe spectroscopy. A femtosecond pulse first excites the heterostructure, and the photo-induced changes in the reflection spectrum ($\Delta R/R$) are probed by a laser-generated supercontinuum light after controlled time delays. For atomically thin heterostructures on a transparent sapphire substrate, the reflection change $\Delta R/R$ is directly proportional to the change in absorption coefficient[31,32]. MoS_2 and WS_2

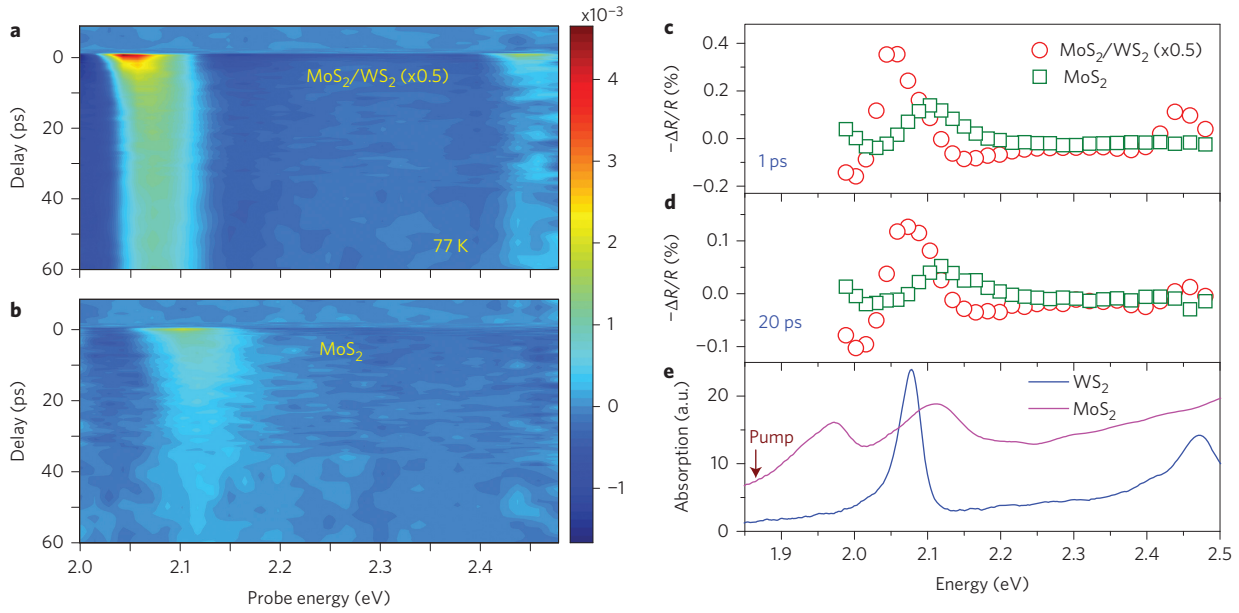

Figure 3 | Transient absorption spectra of MoS_2/WS_2 heterostructures. a,**b**, Two-dimensional plots of transient absorption spectra at 77 K from a MoS_2/WS_2 heterostructure (**a**) and an isolated MoS_2 monolayer (**b**) upon excitation of the MoS_2 A-exciton transitions. The horizontal axis, vertical axis and colour scale represent the probe photon energy, pump–probe time delay and the transient absorption signal, respectively. Positive signals indicate a pump-induced decrease in absorption. **c**,**d**, Transient absorption spectra for MoS_2/WS_2 (red circles) and MoS_2 (green squares) at 1 ps and 20 ps pump–probe delays, respectively. **e**, Linear absorption spectra of monolayers of MoS_2 (magenta line) and WS_2 (blue line). Although only MoS_2 A-exciton transitions are optically excited, transient absorption spectra in the MoS_2/WS_2 heterostructure are dominated by a resonance feature (red circles in **c** and **d**) corresponding to the WS_2 A-exciton transition (blue line in **e**), which is clearly distinguishable from the resonance feature corresponding to the MoS_2 B-exciton transition in an isolated MoS_2 monolayer (green squares in **c** and **d** and magenta line in **e**). This unambiguously demonstrates efficient hole transfer from the photoexcited MoS_2 layer to the WS_2 layer in MoS_2/WS_2 heterostructures.

monolayers have distinctly different exciton transitions. We can therefore selectively excite the MoS_2 or WS_2 layers using specific resonant optical excitations and probe the accumulation of electrons and holes in different layers through photo-induced changes in their respective exciton transitions. Specifically, we chose a pump photon energy at 1.86 eV to excite exclusively the A-exciton transition of MoS_2. This pump cannot excite WS_2 directly because the photon energy is far below the absorption threshold of WS_2. We then examined the photo-induced changes of both WS_2 and MoS_2 exciton resonances in transient absorption spectra from 2.0 to 2.5 eV to probe the charge distribution in the heterostructures.

Using a pump fluence of 85 μJ cm^{-2}, A-excitons in MoS_2 with a density $\sim 5 \times 10^{12}$ cm^{-2} are generated immediately after photoexcitation. Figure 3a presents a two-dimensional plot of transient absorption spectra in a MoS_2/WS_2 heterostructure at 77 K, where the colour scale, the horizontal axis and the vertical axis represent the magnitude of $-\Delta R/R$, the probe photon energy and the pump–probe time delay, respectively. The figure shows prominent resonant features in transient absorption centred on 2.06 eV and 2.46 eV, with the higher energy feature several times weaker than the lower energy one. On comparing this with the linear absorption spectra of isolated WS_2 and MoS_2 monolayers in Fig. 3e, we can attribute these two resonant features, respectively, to the A- and B-exciton transitions in WS_2, although the WS_2 layer is not excited by the pump. To better understand the transient absorption spectra in MoS_2/WS_2 heterostructures, we also performed control experiments for isolated WS_2 and MoS_2 monolayers. In bare WS_2 monolayers no pump-induced signal can be observed above the noise level, consistent with the fact that no direct absorption can take place in WS_2 (Supplementary Section 5). In isolated MoS_2 monolayers, pump-induced absorption changes in our spectral range are centred at 2.11 eV (Fig. 3b), corresponding to the B-exciton transition of MoS_2. Figure 3c,d presents detailed comparisons of the transient absorption spectra in a MoS_2/WS_2 heterostructure and an isolated MoS_2 monolayer at pump–probe time delays of 1 ps (Fig. 3c) and 20 ps (Fig. 3d). Although the resonant features at 2.06 eV for the heterostructure and at 2.11 eV for monolayer MoS_2 are close in energy, they are clearly distinguishable and match well with the A-exciton in WS_2 and B-exciton in MoS_2 in the absorption spectra (Fig. 3e), respectively. In addition, the transient absorption signal at the WS_2 A-exciton transition in the heterostructure is stronger in magnitude and has a narrower spectral width and a slower decay time constant.

Our transient absorption measurements of MoS_2/WS_2 heterostructures establish unambiguously that optical excitation in MoS_2 leads to strong modification of exciton transitions in WS_2, which has a larger optical bandgap. This provides direct evidence of efficient charge separation in photoexcited MoS_2/WS_2 heterostructures (Fig. 1a): electron–hole pairs are initially created in the MoS_2 layer, but holes quickly transfer to the WS_2 layer due to the type II band alignment, while electrons stay in the MoS_2 layer. The photoexcited electrons in MoS_2 and holes in WS_2 lead to a strong transient absorption signal for exciton transitions in both MoS_2 and WS_2. Transient absorption signals are strongest for the A-excitons due to their sharper resonances and efficient photobleaching effects from Pauli blocking, but B-exciton transitions are also affected. Consequently, the transient absorption spectra in MoS_2/WS_2 heterostructures are dominated by the A-exciton transition in WS_2. Photo-induced changes of B-exciton transitions in the MoS_2/WS_2 heterostructure (Fig. 3a) and in the MoS_2 monolayer (Fig. 3b) can also be identified, but they are significantly weaker than that of A-exciton transitions. Room-temperature data show similar trends (Supplementary Section 6).

The rise time of the WS_2 A-exciton transient absorption signal directly probes the hole transfer dynamics from the MoS_2 layer, because this signal exists only after hole transfer, and not right at

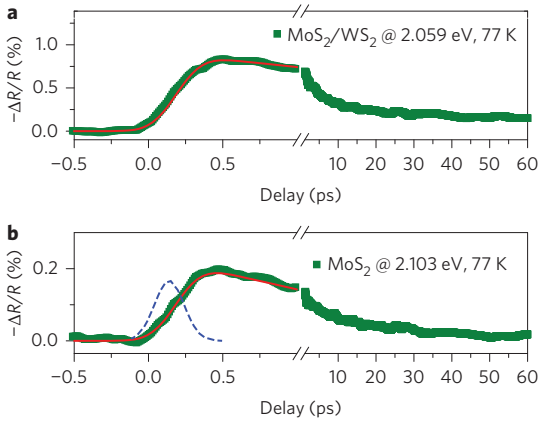

Figure 4 | Ultrafast hole transfer dynamics from vertical cuts in Fig. 3a,b. **a**, Evolution of transient absorption signals at the WS_2 A-exciton resonance in the MoS_2/WS_2 heterostructure. **b**, Dynamic evolution of transient absorption signals at the MoS_2 B-exciton resonance in the isolated MoS_2 monolayer. Both signals show almost identical ultrafast rise times, limited by the laser pulse duration of ~250 fs. By convoluting the instrument response function (blue dashed line in **b**) and an instantaneous response in MoS_2, we can reproduce the ultrafast dynamics in the MoS_2 monolayer (red trace in **b**). Similar convolution shows that the rise time in the MoS_2/WS_2 monolayer is ~25 fs (red trace in **a**) and has an upper limit of 50 fs. This demonstrates that holes can transfer from the photoexcited MoS_2 layer to the WS_2 layer in the MoS_2/WS_2 heterostructure within 50 fs.

the excitation of MoS_2. Figure 4 presents the dynamic evolution of the WS_2 A-exciton resonance in the MoS_2/WS_2 heterostructure (Fig. 4a), which can be compared to the transient absorption signal for the B-exciton resonance in an isolated MoS_2 monolayer (Fig. 4b). We found that the rise times in both signals are almost identical, limited by the laser pulse duration of ~250 fs. In Fig. 4b, the MoS_2 monolayer is directly pumped and the photo-induced signal should appear instantaneously. (The rise times of pump-induced A- and B-exciton signals in MoS_2 have indistinguishable behaviour, as shown in Supplementary Section 8.) We could reproduce the ultrafast dynamics in the MoS_2 monolayer in Fig. 4b by convoluting the instrument response function (blue dashed curve in Fig. 4b) with an instantaneous response in MoS_2. Using the same instrument response function for time convolution, we can then reproduce the experimentally observed signal in the heterostructure with a rise time shorter than 50 fs (red line in Fig. 4a). Our results therefore show that holes are transferred from the MoS_2 layer to the WS_2 layer within 50 fs after optical excitation of the MoS_2/WS_2 heterostructure, a remarkably fast rate. Similar ultrafast hole transfer also takes place at room temperature, as shown in Supplementary Section 7. This hole transfer time is much shorter than the exciton lifetime and most other dynamic processes in MX_2 monolayers, which are on the order of several to tens of picoseconds[33]. Electrons and holes can therefore be efficiently separated into different layers immediately after their generation. Consequently, photoluminescence from MoS_2 and WS_2 exciton resonances will be strongly quenched, as we observed previously.

Our experimental data establish that charge separation in MoS_2/WS_2 heterostructures is very efficient, although the band offset between MoS_2 and WS_2 is smaller than the predicted exciton binding energy in monolayer MX_2. Energetically uncorrelated free electrons and holes in separated MoS_2 and WS_2 layers cannot be produced through the excitation of MoS_2 A-excitons. However, the MoS_2 and WS_2 layers are only separated from each other by ~0.62 nm (ref. 13), suggesting that even for layer-separated electrons and holes, strong Coulomb interactions can lead to bound exciton states. These exciton states with electrons and holes residing in different layers can be energetically favourable compared to an exciton confined to only the MoS_2 layer, and are likely to be responsible for the efficient charge separation observed in MoS_2/WS_2 heterostructures. Such bounded excitons with an electron and hole in different materials, known as charge transfer excitons (CTCs), have also been investigated in other type II heterojunctions, such as molecular donor/acceptor interfaces in the context of organic photovoltaics[21–24,34].

The observed sub-50 fs hole transfer time is remarkably short considering that the MoS_2 and WS_2 layers are twisted relative to each other and are coupled by relatively weak van der Waals interactions. One factor contributing to the ultrafast charge transfer rate in atomically thin heterostructures is the close proximity of the two heterolayers, because electrons or holes only need to move less than 1 nm vertically for the charge transfer process to happen. Still, the 50 fs hole transfer time for van der Waals heterostructures is fast. A microscopic understanding of this ultrafast hole transfer in MX_2 heterostructures requires detailed theoretical studies to examine the hybridization of electronic states in twisted heterolayers and the dynamic evolution of photoexcited states due to electron–phonon and electron–electron interactions. For example, because MoS_2/WS_2 heterostructures are extended crystalline two-dimensional layers, resonant charge transfer has to satisfy both energy and momentum conservations, and electronic coupling between states with different momenta in the Brillouin zone can vary significantly. It is known that for MoS_2 bilayers, electronic coupling at the K point in the Brillouin zone is weak. Electron wavefunction hybridization at the Γ point, however, is much stronger, which leads to a rise in Γ point valence band and an indirect bandgap in bilayer MoS_2 (refs 17,18). Electronic coupling between incommensurate MoS_2 and WS_2 can play an important role in the charge transfer dynamics of twisted MoS_2/WS_2 heterostructures, the behaviour of which has been little studied to date. Because van der Waals heterostructures have atomically sharp interfaces with no dangling bonds and well-defined optical resonances, they provide an ideal model system for further experimental and theoretical investigations of interfacial charge transfer processes and charge transfer exciton states.

The ultrafast charge transfer process in atomically thin MX_2 heterostructures has important implications for photonic and optoelectronic applications. MX_2 semiconductors have extremely strong optical absorption, and have been considered previously for photodetectors[2,3,11], photovoltaics[35] and photocatalysis[36]. Compared with organic photovoltaic materials, these two-dimensional layers have a crystalline structure and better electrical transport properties. Our studies here show that the type II MX_2 heterostructures also exhibit a femtosecond charge transfer rate, which provides an ideal way to spatially separate electrons and holes for electrical collection and utilization.

In summary, we have demonstrated, for the first time, efficient charge transfer in MoS_2/WS_2 heterostructures through combined photoluminesence mapping and transient absorption measurements. We have quantitatively determined the ultrafast hole transfer time to be less than 50 fs. Our study suggests that MX_2 heterostructures, with their remarkable electrical and optical properties and the rapid development of large-area synthesis, hold great promise for future optoelectronic and photovoltaic applications.

Methods

MX_2 monolayer growth. Monolayer MoS_2 was grown by CVD on 285 nm SiO_2/Si substrates[25]. Substrates were loaded into a 1-inch CVD furnace and placed face down above a ceramic boat containing 4.2 mg of MoO_3 (≥99.5%, Sigma-Aldrich). A crucible containing 150 mg of sulphur (≥99.5%, Sigma-Aldrich) was placed upstream. CVD growth was performed at atmospheric pressure with flowing ultrahigh-purity nitrogen. Tuning the sulphur concentration can roughly modify the nucleation density and control the transition of triangular single crystals to a large-area monolayer.

Large-area WS_2 monolayer was grown on sapphire substrates by CVD[26]. A multi-temperature-zone tube furnace (Lindberg/Blue M) equipped with a 1-inch-diameter quartz tube was used for growth. Sulphur powder was mildly sublimated at ~100 °C and placed outside the hot zone. WO_3 powder (Alfa Aesar, purity 99.9%)

and sapphire substrates (⟨0001⟩ oriented single crystals) were successively placed in the hot centre. We used argon (flow rate 80 s.c.c.m.) or mixed argon and hydrogen gas (flow rates of 80 and 10 s.c.c.m., respectively) to carry WO_{3-x} vapour species to the downstream substrates. The growth pressure was set at 30 Pa. Growth temperature was set at ~900 °C and growth time at ~60 min.

Heterostructure preparation. The heterostructure was prepared by transferring[25] monolayer MoS_2 onto monolayer WS_2 on sapphire. The CVD-grown MoS_2 single layer (described above) on SiO_2/Si was spin-coated with poly(methyl methacrylate) (PMMA) (A4) at 4,000 r.p.m. for 60 s. The PMMA/MoS_2 film was separated from the substrate (SiO_2/Si) by KOH etching (1 mol l^{-1}) at 80 °C. The film was transferred to deionized water beakers to dilute KOH residue under MoS_2. It was then transferred onto CVD-grown WS_2 on a sapphire substrate (described above) and soaked in acetone to dissolve the PMMA. Finally, the heterostructure sample was annealed at an elevated temperature in vacuum (Supplementary Section 3). Note there is no polymer between the MoS_2 and WS_2 layers in the sample after PMMA transfer (PMMA was on top of the top layer), so they can form fairly good contact.

Photoluminescence and Raman measurements. For photoluminescence mapping we used a 532 nm laser (photon energy of 2.33 eV) to excite the isolated monolayers of MoS_2 and WS_2 and the MoS_2/WS_2 heterostructures. The laser beam was focused to a diffraction-limited spot (diameter, ~1 μm) and the photoluminescence collected in reflection geometry with a confocal microscope. A monochrometer and a liquid-nitrogen-cooled charge-coupled device (CCD) were used to record the photoluminescence spectra. Two-dimensional photoluminescence mapping was carried out by scanning the computer-controlled piezoelectric stage. For Raman measurements we used a 488 nm excitation laser.

Linear absorption spectra. A supercontinuum laser (Fianium SC450) was used as a broadband light source. The laser was focused at the sample with ~2 μm beam size and the reflection signal R collected via confocal microscopy and analysed by a spectrometer equipped with a one-dimensional CCD array. Reference spectrum R_0 was taken on the sapphire substrate near the sample (isolated MoS_2, isolated WS_2 and heterostructure). The normalized difference signal $(R - R_0)/R_0$ is directly proportional to the linear absorption from atomically thin layers on sapphire[31,32].

Pump–probe measurement. Femtosecond pulses at 1,026 nm were generated by a regenerative amplifier seeded by a mode-locked oscillator (Light Conversion PHAROS). The femtosecond pulses (at a repetition rate of 150 kHz and a pulse duration of ~250 fs) were split into two parts. One was used to pump an optical parametric amplifier to generate tunable excitation laser pulses, and the other was focused into a sapphire crystal to generate a supercontinuum white light (~500–900 nm) for probe pulses. The pump and probe beams were focused at the sample with diameters of ~50 μm and ~25 μm, respectively. The probe light was detected by a high-sensitivity photomultiplier after wavelength selection through a monochrometer with a spectral resolution of 1 nm. The pump–probe time delay was controlled by a motorized delay stage and the pump–probe signal was recorded using lock-in detection with a chopping frequency of 1.6 kHz.

Received 6 February 2014; accepted 16 July 2014; published online 24 August 2014

References

1. Geim, A. K. & Grigorieva, I. V. Van der Waals heterostructures. *Nature* **499,** 419–425 (2013).
2. Britnell, L. *et al.* Strong light–matter interactions in heterostructures of atomically thin films. *Science* **340,** 1311–1314 (2013).
3. Yu, W. J. *et al.* Highly efficient gate-tunable photocurrent generation in vertical heterostructures of layered materials. *Nature Nanotech.* **8,** 952–958 (2013).
4. Yankowitz, M. *et al.* Emergence of superlattice Dirac points in graphene on hexagonal boron nitride. *Nature Phys.* **8,** 382–386 (2012).
5. Ponomarenko, L. a *et al.* Cloning of Dirac fermions in graphene superlattices. *Nature* **497,** 594–597 (2013).
6. Hunt, B. *et al.* Massive Dirac fermions and Hofstadter butterfly in a van der Waals heterostructure. *Science* **340,** 1427–1430 (2013).
7. Dean, C. R. *et al.* Hofstadter's butterfly and the fractal quantum Hall effect in moiré superlattices. *Nature* **497,** 598–602 (2013).
8. Britnell, L. *et al.* Field-effect tunneling transistor based on vertical graphene heterostructures. *Science* **335,** 947–950 (2012).
9. Choi, M. S. *et al.* Controlled charge trapping by molybdenum disulphide and graphene in ultrathin heterostructured memory devices. *Nature Commun.* **4,** 1624 (2013).
10. Jones, A. M. *et al.* Spin–layer locking effects in optical orientation of exciton spin in bilayer WSe_2. *Nature Phys.* **10,** 1–5 (2014).
11. Lopez-Sanchez, O., Lembke, D., Kayci, M., Radenovic, A. & Kis, A. Ultrasensitive photodetectors based on monolayer MoS_2. *Nature Nanotech.* **8,** 497–501 (2013).
12. Gong, C. *et al.* Band alignment of two-dimensional transition metal dichalcogenides: application in tunnel field effect transistors. *Appl. Phys. Lett.* **103,** 053513 (2013).
13. Komsa, H. & Krasheninnikov, A. Electronic structures and optical properties of realistic transition metal dichalcogenide heterostructures from first principles. *Phys. Rev. B* **88,** 085318 (2013).
14. Kang, J., Tongay, S., Zhou, J., Li, J. & Wu, J. Band offsets and heterostructures of two-dimensional semiconductors. *Appl. Phys. Lett.* **102,** 012111 (2013).
15. Terrones, H., López-Urías, F. & Terrones, M. Novel hetero-layered materials with tunable direct band gaps by sandwiching different metal disulfides and diselenides. *Sci. Rep.* **3,** 1549 (2013).
16. Kosmider, K. & Fernandez-Rossier, J. Electronic properties of the MoS_2-WS_2 heterojunction. *Phys. Rev. B* **87,** 075451 (2013).
17. Mak, K. F., Lee, C., Hone, J., Shan, J. & Heinz, T. F. Atomically thin MoS_2: a new direct-gap semiconductor. *Phys. Rev. Lett.* **105,** 136805 (2010).
18. Splendiani, A. *et al.* Emerging photoluminescence in monolayer MoS_2. *Nano Lett.* **10,** 1271–1275 (2010).
19. Berkelbach, T. C., Hybertsen, M. S. & Reichman, D. R. Theory of neutral and charged excitons in monolayer transition metal dichalcogenides. *Phys. Rev. B* **88,** 045318 (2013).
20. Qiu, D. Y., da Jornada, F. H. & Louie, S. G. Optical spectrum of MoS_2: many-body effects and diversity of exciton states. *Phys. Rev. Lett.* **111,** 216805 (2013).
21. Grancini, G., Maiuri, M. & Fazzi, D. Hot exciton dissociation in polymer solar cells. *Nature Mater.* **12,** 29–33 (2013).
22. Jailaubekov, A. E. *et al.* Hot charge-transfer excitons set the time limit for charge separation at donor/acceptor interfaces in organic photovoltaics. *Nature Mater.* **12,** 66–73 (2013).
23. Kaake, L. G., Moses, D. & Heeger, A. J. Coherence and uncertainty in nanostructured organic photovoltaics. *J. Phys. Chem. Lett.* **4,** 2264–2268 (2013).
24. Gélinas, S. *et al.* Ultrafast long-range charge separation in organic semiconductor photovoltaic diodes. *Science* **343,** 512–516 (2014).
25. Van der Zande, A. M. *et al* Grains and grain boundaries in highly crystalline monolayer molybdenum disulphide. *Nature Mater.* **12,** 554–561 (2013).
26. Zhang, Y. *et al.* Controlled growth of high-quality monolayer WS_2 layers on sapphire and imaging its grain boundary. *ACS Nano* **7,** 8963–8971 (2013).
27. Lee, C. *et al.* Anomalous lattice vibrations of single-and few-layer MoS_2. *ACS Nano* **4,** 2695–2700 (2010).
28. Berkdemir, A. *et al.* Identification of individual and few layers of WS_2 using Raman spectroscopy. *Sci. Rep.* **3,** 1755 (2013).
29. Luo, X. *et al.* Effects of lower symmetry and dimensionality on Raman spectra in two-dimensional WSe_2. *Phys. Rev. B* **88,** 195313 (2013).
30. Terrones, H. *et al.* New first order Raman-active modes in few layered transition metal dichalcogenides. *Sci. Rep.* **4,** 4215 (2014).
31. Wang, F. *et al.* Gate-variable optical transitions in graphene. *Science* **320,** 206–209 (2008).
32. Mak, K. F. *et al.* Measurement of the optical conductivity of graphene. *Phys. Rev. Lett.* **101,** 196405 (2008).
33. Shi, H. *et al.* Exciton dynamics in suspended monolayer and few-layer MoS_2; 2D crystals. *ACS Nano* **7,** 1072–1080 (2013).
34. Zhu, X., Yang, Q. & Muntwiler, M. Charge-transfer excitons at organic semiconductor surfaces and interfaces. *Acc. Chem. Res.* **42,** 1779–1787 (2009).
35. Gourmelon, E. *et al.* MS_2 (M = W, Mo) photosensitive thin films for solar cells. *Sol. Energy Mater. Sol. Cells* **46,** 115–121 (1997).
36. Ho, W., Yu, J. C., Lin, J., Yu, J. & Li, P. Preparation and photocatalytic behavior of MoS_2 and WS_2 nanocluster sensitized TiO_2. *Langmuir* **20,** 5865–5869 (2004).

Acknowledgements

Optical measurements and MoS_2 growth were supported by the Office of Basic Energy Science, Department of Energy (contract no. DE-SC0003949, Early Career Award; contract no. DE-AC02-05CH11231, Materials Science Division). The WS_2 growth part was supported financially by the National Natural Science Foundation of China (grants nos. 51222201, 51290272) and the Ministry of Science and Technology of China (grant no. 2011CB921903). F.W. acknowledges support from a David and Lucile Packard fellowship. The authors thank K. Liu and Y. Chen for help in sample characterization and L. Ju for providing the evaporation mask.

Author contributions

F.W. conceived and supervised the experiment. X.H., J.K. and S-F.S. carried out photoluminescence and pump–probe measurements. Y.S., S.T. and J.W. grew CVD monolayer MoS_2. Y.Z. and Y.F.Z. grew CVD monolayer WS_2. J.K., X.H. and S-F.S prepared the heterostructure sample. X.H., J.K., S-F.S. and C.J. performed data analysis. All authors discussed the results and wrote the manuscript.

Additional information

Supplementary information is available in the online version of the paper. Reprints and permissions information is available online at www.nature.com/reprints. Correspondence and requests for materials should be addressed to F.W.

Competing financial interests

The authors declare no competing financial interests.